

Transport and diffusion enhancement in non-Gaussian correlated ratchets

Govind Paneru^{1,2}, Jin Tae Park^{1,2}, and Hyuk Kyu Pak^{1,2*}

¹Center for Soft and Living Matter, Institute for Basic Science (IBS), Ulsan 44919, Republic of Korea

²Department of Physics, Ulsan National Institute of Science and Technology, Ulsan 44919, Republic of Korea

(Dated: April 20, 2021)

Living cells are known to generate non-Gaussian active fluctuations that are significantly larger than thermal fluctuations owing to various metabolic activities. Understanding the effect of active fluctuations on various physicochemical processes, such as the transport of molecular motors, is a fundamental problem in nonequilibrium physics. Therefore, we experimentally and numerically study an active Brownian ratchet comprising a colloidal particle in an optically generated asymmetric periodic potential driven by non-Gaussian noise with finite-amplitude active bursts, each arriving at random and decaying exponentially. We determine that the particle velocity is maximum for relatively sparse bursts with finite correlation time and non-Gaussian distribution. These occasional kicks are more efficient for transport and diffusion enhancement of the particle, compared to the incessant kicks of active Ornstein–Uhlenbeck noise. The ratchet reverses its transport direction only when the noise correlation time is shorter than the thermal relaxation time, suggesting possible application in nanoparticle separation.

1. Introduction

Brownian ratchets^{1–4}, when driven by nonequilibrium fluctuations, can induce the directed transport of diffusive particles in asymmetric potentials. They are used as models for biological transport and nanotechnology applications, such as particle separation and the design of submicron-scale motors^{3–10}. Nonequilibrium fluctuations are generated either from nonequilibrium chemical reactions, such as ATP hydrolysis, or externally through the time-dependent perturbation of the ratchet potential. Accordingly, several Brownian ratchet models have been proposed⁴, and the conditions for their optimal operation have been studied^{4,11,12}. Recent single-molecule studies have revealed that chemically driven molecular motors utilize the input chemical energy for cargo transport by applying mechanical forces on their tracks^{13–15}. However, the molecular motors within a living cell operate in the cell's active environment, which produces active fluctuations larger than thermal fluctuations¹⁶. It is being investigated whether these active fluctuations enhance the performance of individual motors¹⁷.

Correlated ratchets are a special class of Brownian ratchets that consider the diffusion and transport of Brownian particles in asymmetric periodic potentials in the presence of correlated active noise⁴. The correlated ratchets theoretically realized previously consider the motion of a Brownian particle in the presence of exponentially correlated Gaussian noise (active Ornstein–Uhlenbeck (OU) noise)^{4,18,19}, which is a continuous kicking model where the particle position always follows a Gaussian distribution. These studies suggest that OU noise-driven ratchets have low velocities, particularly when the active noise strength is weaker than the thermal strength. Active fluctuations in living cells are because of the activity of the molecular motors present in the

cytoskeletal networks^{16,17}. When fueled by ATP supply, the motors fire at a discrete rate following the Poisson process to generate energy in the form of active bursts, most of which dissipate in the medium. As a result, the displacement of the embedded passive particles shows a non-Gaussian distribution with exponential side tails^{20,21}. Here, we model such non-Gaussian fluctuations in the form of exponentially correlated Poisson noise (ECPN), which is generated numerically by applying a finite response filter to white Poisson noise. It includes finite-amplitude active bursts, each arriving at a random interval following the Poisson counting process and decaying exponentially with the finite correlation time. Our model can generate both non-Gaussian and Gaussian correlated noise by adjusting the noise parameters, which become delta-correlated Poisson and Gaussian white noise under the limiting cases. Hence, it resembles the active fluctuations of various nonequilibrium stochastic systems, such as intracellular environments^{20,22}, the active baths of biological and synthetic swimmers^{23–30}, and glassy systems³¹.

In this study, we realize an active Brownian ratchet comprising a colloidal particle in an optically generated periodic potential driven by ECPN noise with tunable parameters. Experimentally, the construction of the ratchet potential and insertion of active noise is performed through the high-precision and ultrafast measurement of the particle position in the optical trap followed by the feedback control that considers the rapid shift of the trap center. The average velocity of the particle is optimal for a finite correlation time, where each active burst decays fully before the arrival of another burst. This suggests that the discrete firing of molecular motors should be an optimized strategy for cargo transport. We also found that the thermal relaxation time dictates the particle transport direction, indicating that the

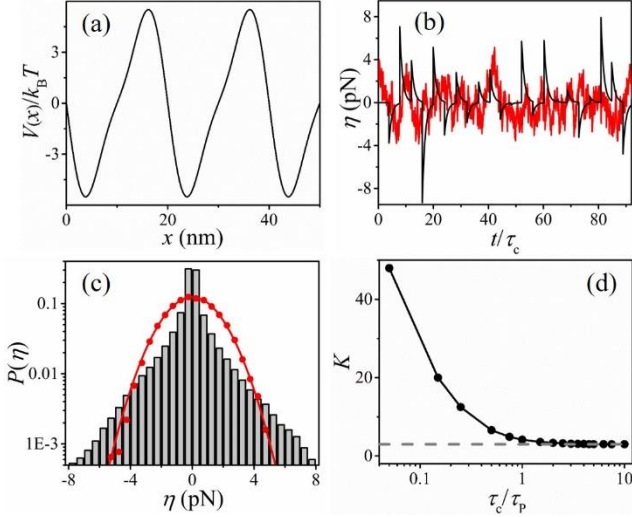


Fig. 1 Schematic of the periodic potential and plot of the active noise: (a) Plot of the asymmetric periodic potential $V(x)$ in Eq. (1) as a function of position x with $L = 20$ nm and $V_0 = 5k_B T$. As the lhs of the each potential well is steeper than the rhs, the natural ratchet direction is along the positive x direction. (b) Traces of the active OU noise (red) and ECPN noise (black) of the same strength $f_{act} = \sqrt{F/(1+\lambda)} = 1.5$ pN and correlation time $\tau_c/\Delta t = 100$, where Δt is the noise input interval, with Poisson parameter $\lambda = 0$ (red, OU) and $\lambda = 400$ (black, ECPN). (c) Probability distribution function of the active noises in panel (b). (d) Kurtosis $K(t)$ as a function of τ_c/τ_p , showing the degree of non-Gaussianity of the ECPN. The horizontal dashed line corresponds to a Gaussian distribution $K = 3$.

particle moves opposite to the natural alignment of the ratchet potential only when the noise correlation time is shorter than the thermal relaxation time of the particle. Furthermore, our parametric studies show that the particle position distribution is always Gaussian. In contrast, the distribution of the particle displacement is non-Gaussian when the noise correlation time is shorter than the average burst interval and the noise strength is greater than the thermal noise strength; otherwise, it follows a Gaussian form. In addition, the non-Gaussianity of active noise leads to pronounced diffusion enhancement.

2. Results

2.1 Active Brownian ratchet

We investigated the one-dimensional motion of a Brownian particle immersed in an active bath of temperature T , diffusing in a spatially asymmetric periodic potential of period L and barrier height $2V_0$ (see Fig. 1(a)):

$$V(x) = -V_0 [\sin(2\pi x/L) + 0.25 \sin(4\pi x/L)]. \quad (1)$$

The motion of the particle is governed by thermal fluctuations $\xi(t)$ due to the solvent molecules and active

fluctuations $\eta(t)$ due to the active noise source in the solution. The equation of motion for particle position x is described by the overdamped Langevin equation:

$$\gamma \frac{dx}{dt} = -\frac{\partial V(x)}{\partial x} + \xi(t) + \eta(t), \quad (2)$$

where γ is the Stokes friction coefficient, which represents the solvent viscosity. The thermal fluctuations $\xi(t)$ are modeled by Gaussian white noise of zero mean $\langle \xi(t) \rangle = 0$ and a correlation function $\langle \xi(t)\xi(s) \rangle = 2\gamma^2 D_{th} \delta(t-s)$. Here $D_{th} = k_B T / \gamma$ is the free diffusion coefficient of the particle in the thermal bath alone. The characteristic thermal relaxation time of the particle in the potential well is $\tau_r \approx 0.08(\gamma L^2 / V_0)^4$.

The active fluctuations $\eta(t)$ are modeled by exponentially correlated finite-amplitude random kicks with correlation time τ_c acting on the system at an average Poisson interval τ_p following the Poisson process. $\eta(t)$ is generated numerically from Poisson white noise, $\xi_{PN}(t) = \sum_{i=1}^{N(t)} y_i \delta(t-t_i)$, where t_i are the arrival time of a Poisson counting process $N(t)$ with mean arrival time τ_p and y_i are Gaussian random variables with variance F , using the recursion relation³²,

$$\eta_n = \eta_0 \exp(-n/\tau_c) + \sqrt{1 - \exp(-2/\tau_c)} \sum_{i=1}^n (\xi_{PN})_i \exp(-(n-i)/\tau_c). \quad (3)$$

Equation (3) generates a sequence of ECPN of zero mean, $\langle \eta(t) \rangle = 0$, and the following correlation function:

$$\langle \eta(t)\eta(s) \rangle = \frac{F}{1+\lambda} \exp(-|t-s|/\tau_c). \quad (4)$$

Here, λ is the Poisson parameter that gives the average number of waiting events between successive kicks. Therefore, the average time between two consecutive kicks is given by $\tau_p = \lambda \Delta t$, with a noise input interval Δt .

$f_{act} \equiv \sqrt{F/(1+\lambda)}$ characterizes the strength of the active noise. When $\lambda = 0$ (which corresponds to $\tau_p = 0$), our noise model follows active OU noise with vanishing mean $\langle \eta(t) \rangle = 0$ and correlation function $\langle \eta(t)\eta(s) \rangle_{OU} = (\gamma^2 D_{act} / \tau_c) \exp(-|t-s|/\tau_c)$. The variance of the active burst F can then be expressed in terms of the active diffusion coefficient D_{act} and noise correlation time τ_c as $F = \gamma^2 D_{act} / \tau_c$. For direct comparison, the time traces of the ECPN as well as OU noise of the same strength and

correlation time are depicted in Fig. 1(b). For $\tau_c \lesssim \tau_p$, each active burst decays completely on an average before the arrival of another burst, and the ECPN follows a non-Gaussian distribution with exponential side-tails (the black bars Fig. 1(c)). The degree of non-Gaussianity of the probability distribution function (PDF) of the noise can be quantified by the kurtosis

$K(t) = \langle [\eta(t) - \langle \eta(t) \rangle]^4 \rangle / \langle [\eta(t) - \langle \eta(t) \rangle]^2 \rangle^2$. For a Gaussian distribution $K = 3$. K decreases with the increase in τ_c and saturates to three for $\tau_c \gtrsim 5\tau_p$ (Fig. 1(d)).

2.2 Generation of periodic potentials

The periodic potential indicated in Eq. (1) is generated using the optical feedback trap technique³³⁻³⁹. Here, we consider a colloidal particle (2 μm diameter polystyrene spheres) trapped in the harmonic potential of an optical trap, $V_{\text{op}}(x, t) = (k/2)(x - x_c(t))^2$, where x_c is the position of the trap center (the experimental setup is described in the Methods section). A quadrant photodiode (QPD) measures the particle position x and sends the data to a field-programmable gate array (FPGA) board at a sampling time $\Delta t \approx 10 \mu\text{s}$ using a custom-written LabVIEW FPGA program. The FPGA board computes the feedback force $f_{\text{fd}} = -\partial_x V(x)$ necessary to generate the periodic potential in Eq. (1). Numerically generated active noise $\eta(t)$ (Eq. (3)) is added to the feedback force to impose an active force on the particle (the noise input interval is thus essentially the same as the sampling time $\Delta t \approx \tau_p/\lambda$). The resultant feedback force $f_{\text{fd}}(t) + \eta(t)$ is applied to the particle in the form of an optical force by a practically instantaneous shift of the trap center to $x_c(t) = x(t) - (1/k)\partial_x V(x) + \eta(t)/k$. To realize this, the FPGA updates the tuning voltage (equivalent to the resultant force) that is applied to the acousto-optic deflector (AOD) through a radiofrequency (RF) synthesizer driver for steering the laser beam center by $x_c(t)$. On repeatedly performing this procedure, the particle experiences an asymmetric potential and active noise $\eta(t)$ in time.

2.3 Experimental results

The magnitude and direction of the particle velocity depend on the active noise parameters. The number of periods of the asymmetric periodic potential to which the particle is transported is limited by the linear working range of the QPD, for which the optical trap stiffness is constant. This range is approximately $\pm 300 \text{ nm}$ for the current setup. Therefore, starting from the fixed initial location of the trap center $x_c(0)$ and random particle position $x(0) - x_c(0)$, each experimental run records the particle trajectory for a duration t during which the particle is transported by $\pm 300 \text{ nm}$. The particle velocity is then measured using the relation

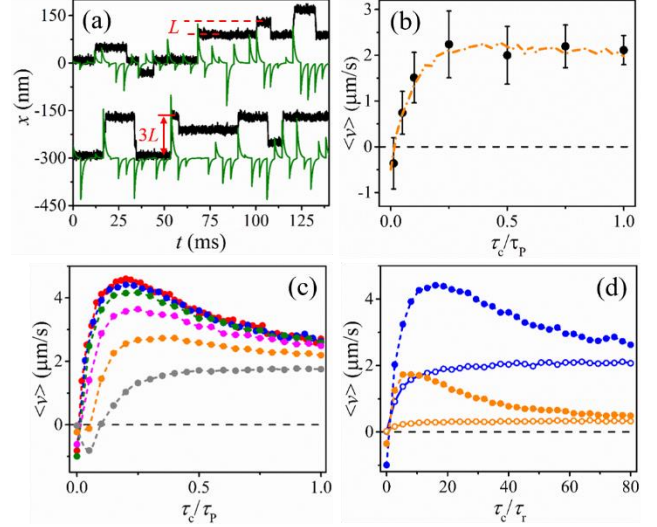


Fig. 2 Measurement of trajectories of the particle position and average velocity: (a, b experimental results): (a) Two trajectories of the particle position (black) for particle motion in a virtual asymmetric periodic potential of period $L = 40 \text{ nm}$ and barrier height $2V_0 = 10k_B T$ in the presence of ECPN noise (olive) of amplitude $f_{\text{act}}/k \approx 35 \text{ nm}$ with the Poisson interval normalized by the thermal relaxation time $\tau_p/\tau_r \approx 33.3$ and correlation time $\tau_c/\tau_p \approx 0.25$. For better visualization, the bottom trajectory is shifted below by 300 nm. (b) Plot of the average velocity $\langle v \rangle$ of the particle as a function of τ_c/τ_p for ECPN of the same noise strength and Poisson interval of panel a. The error bars denote the standard error of the mean. The orange dashed curve is obtained through the numerical simulation of Eq. (2). (c, d numerical results): (c) Plot of the average velocity $\langle v \rangle$ of the particle in steady state as a function of the correlation time normalized with the Poisson interval τ_c/τ_p for ECPN of fixed noise strength $f_{\text{act}} \approx 1.5 \text{ pN}$ and Poisson interval $\tau_p/\tau_r = 6.7$ (gray), 13.3 (orange), 26.7 (magenta), 53.3 (olive), 80 (blue), and 133.3 (red). d Comparison of the ECPN (solid circles) and OU (open circles) noises. Plot of $\langle v \rangle$ as a function of τ_c/τ_r in the presence of ECPN with $\tau_p/\tau_r = 80$ and OU noise of the same strength with $f_{\text{act}} = 1.0 \text{ pN}$ (orange) and 1.5 pN (blue).

$v = (x(t) - x(0))/t$. Similar to previous theoretical studies, we fixed the peak-to-peak barrier height of the periodic potential as $2V_0 \approx 10k_B T$ ⁴. The period of the asymmetric potential in Eq. (1) is selected as $L \approx 40 \text{ nm}$, such that the time scale for the particle to diffuse one period of the potential $\tau_D \approx L^2/D_{\text{th}} \approx 7 \text{ ms}$ is considerably larger than sampling time $\Delta t \approx 10 \mu\text{s}$ (in addition, Δt is smaller than $\tau_r \approx 120 \mu\text{s}$).

The sufficient condition for obtaining a nonvanishing mean velocity in the original Gaussian correlation ratchet involves energy input with finite correlation time¹⁹. The

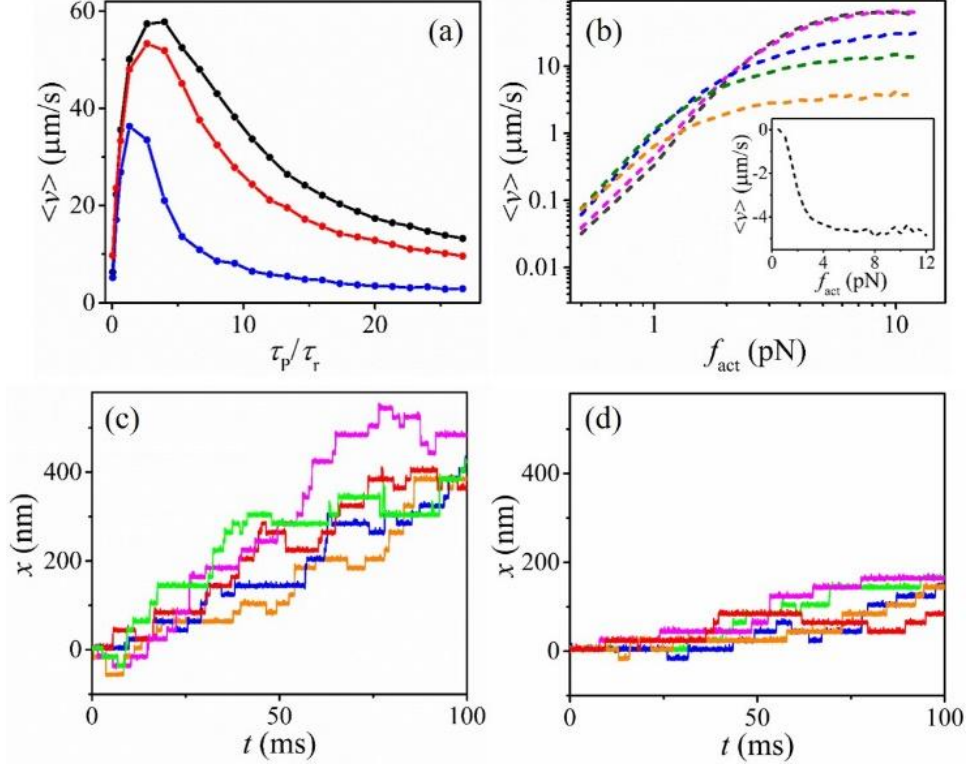


Fig. 3 Average velocity and trajectories of the particle position: (a) Plot of $\langle v \rangle$ as a function of τ_p/τ_r for a fixed active burst strength $\sqrt{F} \approx 60$ pN and $\tau_c/\tau_r = 1.33$ (blue), 4 (red), and 6.7 (black). (b) Plot of $\langle v \rangle$ as a function of the active noise strength f_{act} for fixed $\tau_p/\tau_r = 26.7$ and $\tau_c/\tau_p = 0.05$ (orange), 0.125 (olive), 0.25 (blue), 1 (magenta). The black curve denotes the OU noise case ($\lambda = 0$) with $\tau_c/\tau_r = 26.7$. Inset: Current inversion for $\tau_p/\tau_r = 26.7$ and $\tau_c/\tau_r = 0.07$. (c) Sample trajectories of the particle driven by ECPN noise with $f_{act} \approx 1.5$ pN and $\tau_c/\tau_p = 0.25$. (d) Sample trajectories of the particle with OU noise of the same strength and correlation time as in (c). Due to the large-amplitude discrete bursts of the ECPN, the particle escapes each well faster than that for the relatively smaller magnitude continuous kicks of OU noise where the particle dwells in each well for a relatively longer duration.

energy input lowers the barrier height effectively, while the correlation time allows the particles to diffuse in the direction of the active force. However, because of the asymmetry of the periodic potential, particle transport along the positive x -direction is more favorable. Figure 2(a) compares the two trajectories of a particle diffusing in the asymmetric periodic potential with the corresponding ECPN noise trajectories of strength $f_{act} \approx 1.05$ pN; the Poisson interval normalized with the relaxation time $\tau_p/\tau_r \approx 33.3$ and the correlation time normalized with the Poisson interval $\tau_c/\tau_p \approx 0.25$. A particle diffusing at the bottom of a potential well can cross the potential barrier and move to the neighboring wells when acted upon by an active burst with an amplitude comparable to the thermal strength $f_{th} = \sqrt{\gamma k_b T / \tau_r}$, i.e., $\eta(t) \sim f_{th} \approx 0.8$ pN. For active bursts with greater strength, the particle may even cross several

potential periods, which is evident from some of the large step jumps (see the lower trajectory in Fig. 2(a)).

Figure 2(b) depicts the particle mean velocity $\langle v \rangle$ as a function of τ_c/τ_p for fixed values of $f_{act} \approx 1.05$ pN and $\tau_p/\tau_r \approx 33.3$. The mean velocity was obtained by averaging more than 900 trajectories (the typical velocity distribution is shown in Supplementary Fig. 2). The average velocity increases with the increase in τ_c and reaches near-saturation beyond $\tau_c/\tau_p \approx 0.25$. In contrast, for a shorter correlation time ($\tau_c = 50$ μs in Fig. 2(b)), the average velocity assumes a negative value, which indicates that the particle moves in a direction opposite to that of the natural alignment of the asymmetric potential.

2.4 Numerical results

Due to the limitations in the working region of the QPD, our experimental study could only explore the intermediate time

behavior of particle diffusion. To study the long-time behavior, we solved Eq. (2) numerically using Euler's method. Here, we set the particle diameter to $1 \mu\text{m}$ and the period of the periodic potential $L = 20 \text{ nm}$, such that the thermal relaxation time of the particle is $\tau_r = 15 \mu\text{s}$. Figure 2(c) displays the plot of the average velocity of the particle in steady state $\langle v \rangle = \langle \lim_{t \rightarrow \infty} (x(t) - x(0))/t \rangle$ as a function of τ_c/τ_p for a fixed value of the active noise strength $f_{act} \approx 2 \text{ pN}$. The average was taken over 1,000 trajectories, each with a duration of 150 ms. For a given value of τ_p , the average velocity increases with the increase in τ_c and is maximum near $\tau_c/\tau_p \approx 0.25$, where the active noise still displays highly non-Gaussian behavior (see Fig. 1(d)). The velocity is saturated for $\tau_c \gtrsim \tau_p$ where the active noise is Gaussian-like. For a shorter correlation time ($\tau_c \leq 10 \mu\text{s}$), the average velocity is negative. This agrees with the experimental result in Fig. 2(b) (for the ratchet parameters used in the experiment, our numerical results show that the particle velocity is negative when $\tau_c \leq 100 \mu\text{s}$), in predicting that the particle transport direction is controlled by the noise correlation time, particle size, and potential period L . Thus, for the asymmetric potential in Eq. (1), the particle velocity is negative only when $\tau_c < \tau_r$. This also includes the $\tau_c = 0$ limit, which is consistent with prior theoretical prediction that demonstrated current inversion in the presence of symmetric Poisson white noise⁴⁰. Figure 2(c) also illustrates the dependence of the particle velocity on τ_p . The velocity increases with the increase in τ_p and becomes saturated for $\tau_p \gtrsim 5\tau_D$. The distinctive feature of ECPN noise compared to classical OU noise of the same strength is that it can transport particles with notably enhanced velocity (see Fig. 2(d)). Specifically, the smaller the active noise strength, the larger is the difference in the particle velocity between the two noises. For an active noise strength comparable to the thermal noise strength $f_{act} \sim f_{th} \approx 1.6 \text{ pN}$, the particle velocity in the presence of OU noise is an order of magnitude smaller than that of ECPN. In addition, OU noise cannot drive the particles in the negative direction.

Furthermore, we studied the dependence of the particle velocity as a function of the Poisson interval τ_p for a fixed active burst strength \sqrt{F} and noise correlation time τ_c (Fig. 3(a)). At a given \sqrt{F} , the particle velocity generally assumes a bell shape with a maximum at a finite value of τ_p for which the magnitude of the active noise strength becomes $f_{act} \approx 9 \text{ pN}$. Hence, although the strength of the active noise is maximum ($f_{act} \approx \sqrt{F}$) for $\tau_p \approx 0$, the particle velocity is maximum at a finite value of τ_p . Fig. 3(b) displays the plot of the particle velocity as a function of the

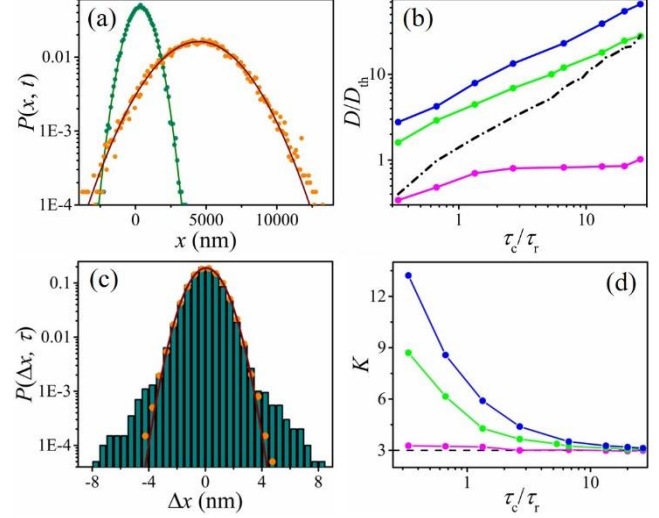


Fig. 4 Steady state probability distribution functions and effective diffusion coefficient: (a) PDF $P(x, t)$ of particle position x at time t for ECPN of fixed strength $f_{act} = 4 \text{ pN}$ and Poisson interval $\tau_p/\tau_r = 26.7$ with $\tau_c/\tau_p = 0.05$ (olive) and 1 (orange). The solid curves are the Gaussian fit of the data. The PDFs are calculated for $t/\tau_r \approx 7000$ for which $\sigma_x^2(t) = 2Dt$ is valid. The distributions are constructed from the end data points of 20,000 trajectories. (b) Plot of the effective diffusion coefficient normalized with the free thermal diffusion coefficient D/D_{th} as a function of τ_c/τ_r for ECPN of fixed Poisson interval $\tau_p/\tau_r = 26.7$ and noise strength $f_{act} = 2$ (magenta), 4 (green), and 5 (blue) pN. The dashed black curve is for OU noise of the same strength ($f_{act} = 4 \text{ pN}$) as that of the green data. (c) PDF $P(\Delta x, \tau)$ for particle displacement $\Delta x = x(t + \tau) - x(t)$ obtained from the like-colored data in panel (a). (d) Kurtosis of $P(\Delta x, \tau)$ vs τ_c/τ_r for like-colored data in panel (b).

active noise strength f_{act} for a fixed τ_p and for different values of τ_c . At each τ_c/τ_p , the particle velocity increases with the magnitude of the active burst \sqrt{F} , except for $\tau_c < \tau_r$ where it assumes a negative value and saturates to a negative value (see inset of Fig. 3(b)). For an active noise strength comparable to the thermal noise strength ($f_{act} \approx f_{th}$), the particle velocity increases with τ_c/τ_p and reaches a maximum near $\tau_c/\tau_p \approx 0.25$, where each active kick decays completely before a new kick arrives ($\tau_c \sim \tau_D$). An additional increase in τ_c has a diminishing return because the particle velocity decreases for longer τ_c and becomes zero for $\tau_c/\tau_p > 1$, where the particle experiences multiple kicks simultaneously (Gaussian limit). Interestingly, for an active noise strength lesser than the thermal noise strength $f_{act} \lesssim f_{th}$, where OU noise can barely transport a particle,

ECPN can transport the particle with a finite velocity; this can also be observed from the particle trajectories (Fig. 3(c) for ECPN and Fig. 3(d) for OU noise). However, for a larger magnitude of the active noise strength ($f_{act} > f_{th}$) and $\tau_c/\tau_p \gtrsim 1$, the particle velocity saturates to the value predicted by OU noise of equal strength and correlation time, suggesting that discrete-pulsed non-Gaussian noise is sufficient for transporting particles at optimal speed.

Next, we show that the ECPN noise with three independently controllable parameters leads to the Brownian, yet non-Gaussian diffusion, where the mean square displacement of the particle scales linearly with time, and the PDF of the position displacement is non-Gaussian⁴¹. For this, we measured the PDF $P(x, t)$ of particle position x at time t in the presence of ECPN of fixed strength $f_{act} = 4$ pN and Poisson interval $\tau_p/\tau_r = 26.7$ (Fig. 4(a)). Similar to OU noise, $P(x, t)$ for ECPN is always Gaussian-like with kurtosis $K(t) \approx 3$. However, the variance of the particle position $\sigma_x^2(t)$ increases with the increase in τ_c . In contrast, for fixed values of the active noise parameters within the limit $t \gg \tau_r$, $\sigma_x^2(t)$ scales linearly with time. Based on this, we can measure the effective diffusion coefficient $D = \lim_{t \rightarrow \infty} \sigma_x^2(t)/2t$ of a particle. For $f_{act} \lesssim f_{th}$, where ECPN can still induce directed motion of the particle, the effective diffusion coefficient is always less than the free thermal diffusion coefficient, $D/D_{th} < 1$ (Fig. 4(b)). For $f_{act} > f_{th}$, the effective diffusion coefficient increases with increase in τ_c , leading to enhanced diffusion. Interestingly, diffusion enhancement for a relatively shorter correlation time is significantly greater than that of OU noise of the same strength and correlation time (see the dashed-dotted black curve in Fig. 4(b)).

We also measured the PDF $P(\Delta x, \tau)$ of particle displacement $\Delta x = x(t + \tau) - x(t)$ for $\tau = \Delta t$ within the limit $t \gg \tau_r$. We found that when the active noise strength is lesser than the thermal strength $f_{act} \lesssim f_{th}$, $P(\Delta x, \tau)$ always exhibits Gaussian behavior ($K \approx 3$) regardless of the values of τ_c and τ_p . In contrast, for $f_{act} > f_{th}$ and $\tau_c < \tau_p$, $P(\Delta x, \tau)$ adopts non-Gaussian behavior, exhibiting a Gaussian shape at the center and an exponentially decaying side-tails (Fig. 4(c)). The degree of non-Gaussianity decreases with the increase in the τ_c/τ_p ratio and assumes a Gaussian form for $\tau_c/\tau_p \gtrsim 1$, as depicted in Fig. 4(d), which shows the kurtosis of the particle position displacement as a function of τ_c/τ_p . Figure 4(d) also shows that for a given value of $\tau_c < \tau_p$, the degree of non-Gaussianity increases with the active noise strength, suggesting that rare active

bursts are responsible for the exponential side-tails in $P(\Delta x, \tau)$.

3. Discussion

In conclusion, we examined an active Brownian ratchet comprising a colloidal particle in an optically generated asymmetric periodic potential in the presence of numerically generated non-Gaussian noise. Generation of the asymmetric periodic potential and insertion of active noise were performed simultaneously using the optical feedback trap technique. We determined that the sufficient condition for optimal velocity and diffusion enhancement was the injection of finite-time-correlated discrete energy pulses rather than the continuous energy supply of OU noise-driven ratchets. This is significant for the active transport of molecular motors within living cells, where the energy input is limited by the ATP concentration resulting in discrete motor firing rates. We demonstrated that the particle position always followed a Gaussian distribution, whereas the particle displacement distribution was non-Gaussian only when the active force strength was greater than the thermal strength, and each active burst decayed before the arrival of another burst. Thus, our noise model is vital in explaining the Brownian, yet non-Gaussian diffusion dynamics observed in various active matter systems⁴¹.

The transport direction of the ratchet was controlled by the active noise correlation time and thermal relaxation time of the particle, i.e., the particle velocity was positive only when the noise correlation time was greater than the thermal relaxation time. This implies that under a fixed substrate potential and active noise parameters, the magnitude and direction of the velocity depend on the particle size. Accordingly, our simple model predicted that the non-Gaussian active fluctuations within living cells would enhance the motion of kinesin motors toward the positive end of the microtubules, whereas for the relatively larger sized dynein motors, it would promote motion in the opposite direction. The prediction that non-Gaussian noise would enhance kinesin motor motion toward the positive end of the microtubule is consistent with a recent study⁴², which showed velocity enhancement for a kinesin motor moving along a microtubule when the cargo (attached bead) was driven by levy noise⁴². However, although a recent study showed that periodic fluctuations enhanced the motion of dynein motors toward the negative end of the microtubules⁴³, whether non-Gaussian active fluctuations enhance their motion is to be researched in future. The findings of this study are crucial for understanding the effect of active fluctuations on nonequilibrium and stochastic processes in various active baths. It can open new avenues for designing efficient synthetic and biological microscale stochastic devices and has technological applications, such as nanoparticle separation¹⁰.

4. Methods

4.1 Experimental setup

The schematic of the optical feedback trap setup is depicted in Supplementary Fig. 1. This is similar to our previous setup⁴⁴, except for the usage of a faster QPD (Thorlabs, PDQ30C) for position detection. A 1064-nm wavelength laser is used to trap the particles. The laser beam is passed through an AOD at the Bragg angle, resulting in maximum power output for the first-order beam. This beam is focused on the sample plane of an optical microscope using a 100X oil immersion objective lens with a high numerical aperture (NA = 1.4). A second laser with a wavelength of 980 nm is used for particle position detection. The particle position is measured by the QPD mounted at the back focal plane of a 1.4 NA condenser lens. The QPD signal is acquired by an FPGA data acquisition board using a custom-written LabVIEW FPGA program. The sample cell includes a highly diluted solution of 2 μm polystyrene spheres suspended in deionized water at room temperature 297 ± 1 K. The trap parameters were calibrated by fitting the probability distribution of the particle position in the thermal equilibrium to the Boltzmann distribution $P(x) = (2\pi\sigma^2)^{-1/2} \exp(-x^2/2\sigma^2)$. The trap stiffness was then estimated as $k \approx 30 \text{ pN}\mu\text{m}^{-1}$ using the equipartition relation $k = k_B T / \sigma^2$.

Acknowledgements

This work was supported by the Institute for Basic Science (Grant No. IBS-R020). We thank Juzar Thingna for useful discussions.

References

- 1 Feynman, R. P., Leighton, R. B. & Sands, M. *The Feynman Lectures on Physics*. (Addison-Wesley Publishing Company, 1964).
- 2 Reimann, P. Brownian motors: noisy transport far from equilibrium. *Physics Reports* **361**, 57-265, doi:[https://doi.org/10.1016/S0370-1573\(01\)00081-3](https://doi.org/10.1016/S0370-1573(01)00081-3) (2002).
- 3 Astumian, R. D. & Hänggi, P. Brownian Motors. *Physics Today* **55**, 33, doi:10.1063/1.1535005 (2002).
- 4 Hänggi, P. & Marchesoni, F. Artificial Brownian motors: Controlling transport on the nanoscale. *Reviews of Modern Physics* **81**, 387-442 (2009).
- 5 van Oudenaarden, A. & Boxer, S. G. Brownian Ratchets: Molecular Separations in Lipid Bilayers Supported on Patterned Arrays. *Science* **285**, 1046-1048, doi:10.1126/science.285.5430.1046 (1999).
- 6 Matthias, S. & Müller, F. Asymmetric pores in a silicon membrane acting as massively parallel brownian ratchets. *Nature* **424**, 53-57, doi:10.1038/nature01736 (2003).
- 7 Mahmud, G. *et al.* Directing cell motions on micropatterned ratchets. *Nature Physics* **5**, 606-612, doi:10.1038/nphys1306 (2009).

- 8 Iino, R., Kinbara, K. & Bryant, Z. Introduction: Molecular Motors. *Chemical Reviews* **120**, 1-4, doi:10.1021/acs.chemrev.9b00819 (2020).
- 9 Astumian, R. D. & Derényi, I. Fluctuation driven transport and models of molecular motors and pumps. *European Biophysics Journal* **27**, 474-489, doi:10.1007/s002490050158 (1998).
- 10 Skaug, M. J., Schwemmer, C., Fringes, S., Rawlings, C. D. & Knoll, A. W. Nanofluidic rocking Brownian motors. *Science* **359**, 1505-1508, doi:10.1126/science.aal3271 (2018).
- 11 Wagoner, J. A. & Dill, K. A. Mechanisms for achieving high speed and efficiency in biomolecular machines. *Proceedings of the National Academy of Sciences* **116**, 5902-5907, doi:10.1073/pnas.1812149116 (2019).
- 12 Astumian, R. D. Irrelevance of the Power Stroke for the Directionality, Stopping Force, and Optimal Efficiency of Chemically Driven Molecular Machines. *Biophys J* **108**, 291-303, doi:<https://doi.org/10.1016/j.bpj.2014.11.3459> (2015).
- 13 Visscher, K., Schnitzer, M. J. & Block, S. M. Single kinesin molecules studied with a molecular force clamp. *Nature* **400**, 184-189, doi:10.1038/22146 (1999).
- 14 Ariga, T., Tomishige, M. & Mizuno, D. Nonequilibrium Energetics of Molecular Motor Kinesin. *Physical Review Letters* **121**, 218101, doi:10.1103/PhysRevLett.121.218101 (2018).
- 15 Mugnai, M. L., Hyeon, C., Hinczewski, M. & Thirumalai, D. Theoretical perspectives on biological machines. *Reviews of Modern Physics* **92**, 025001, doi:10.1103/RevModPhys.92.025001 (2020).
- 16 Mizuno, D., Tardin, C., Schmidt, C. F. & MacKintosh, F. C. Nonequilibrium Mechanics of Active Cytoskeletal Networks. *Science* **315**, 370-373, doi:10.1126/science.1134404 (2007).
- 17 Guo, M. *et al.* Probing the Stochastic, Motor-Driven Properties of the Cytoplasm Using Force Spectrum Microscopy. *Cell* **158**, 822-832, doi:<https://doi.org/10.1016/j.cell.2014.06.051> (2014).
- 18 Magnasco, M. O. Forced thermal ratchets. *Physical Review Letters* **71**, 1477-1481, doi:10.1103/PhysRevLett.71.1477 (1993).
- 19 Bartussek, R., Reimann, P. & Hänggi, P. Precise Numerics versus Theory for Correlation Ratchets. *Physical Review Letters* **76**, 1166-1169, doi:10.1103/PhysRevLett.76.1166 (1996).
- 20 Fodor, É. *et al.* Activity-driven fluctuations in living cells. *EPL (Europhysics Letters)* **110**, 48005, doi:10.1209/0295-5075/110/48005 (2015).
- 21 Shin, K. *et al.* Anomalous Dynamics of in Vivo Cargo Delivery by Motor Protein Multiplexes. *The Journal of Physical Chemistry Letters* **10**, 3071-3079, doi:10.1021/acs.jpcclett.9b01106 (2019).
- 22 Hidalgo-Soria, M. & Barkai, E. Hitchhiker model for Laplace diffusion processes. *Physical Review E* **102**, 012109, doi:10.1103/PhysRevE.102.012109 (2020).
- 23 Wu, X.-L. & Libchaber, A. Particle Diffusion in a Quasi-Two-Dimensional Bacterial Bath. *Physical Review Letters* **84**, 3017-3020, doi:10.1103/PhysRevLett.84.3017 (2000).
- 24 Kurtuldu, H., Guasto, J. S., Johnson, K. A. & Gollub, J. P. Enhancement of biomixing by swimming algal cells in

- two-dimensional films. *P Natl Acad Sci USA* **108**, 10391-10395, doi:10.1073/pnas.1107046108 (2011).
- 25 Goldstein, R. E., Polin, M. & Tuval, I. Noise and Synchronization in Pairs of Beating Eukaryotic Flagella. *Physical Review Letters* **103**, 168103, doi:10.1103/PhysRevLett.103.168103 (2009).
- 26 Dabelow, L., Bo, S. & Eichhorn, R. Irreversibility in Active Matter Systems: Fluctuation Theorem and Mutual Information. *Physical Review X* **9**, 021009, doi:10.1103/PhysRevX.9.021009 (2019).
- 27 Kanazawa, K., Sano, T. G., Cairoli, A. & Baule, A. Loopy Lévy flights enhance tracer diffusion in active suspensions. *Nature* **579**, 364-367, doi:10.1038/s41586-020-2086-2 (2020).
- 28 Bechinger, C. *et al.* Active particles in complex and crowded environments. *Reviews of Modern Physics* **88**, 045006, doi:10.1103/RevModPhys.88.045006 (2016).
- 29 Barkai, E. & Burov, S. Packets of Diffusing Particles Exhibit Universal Exponential Tails. *Physical Review Letters* **124**, 060603, doi:10.1103/PhysRevLett.124.060603 (2020).
- 30 Leptos, K. C., Guasto, J. S., Gollub, J. P., Pesci, A. I. & Goldstein, R. E. Dynamics of Enhanced Tracer Diffusion in Suspensions of Swimming Eukaryotic Microorganisms. *Physical Review Letters* **103**, 198103, doi:10.1103/PhysRevLett.103.198103 (2009).
- 31 Chaudhuri, P., Berthier, L. & Kob, W. Universal Nature of Particle Displacements close to Glass and Jamming Transitions. *Physical Review Letters* **99**, 060604, doi:10.1103/PhysRevLett.99.060604 (2007).
- 32 Deserno, M. How to generate exponentially correlated Gaussian random numbers. [https://www.cmu.edu/biolphys/deserno/pdf/corr_gaussian_random.pdf].
- 33 Paneru, G., Lee, D. Y., Tlusty, T. & Pak, H. K. Lossless Brownian Information Engine. *Physical Review Letters* **120**, 020601 (2018).
- 34 Paneru, G. *et al.* Optimal tuning of a Brownian information engine operating in a nonequilibrium steady state. *Physical Review E* **98**, 052119, doi:10.1103/PhysRevE.98.052119 (2018).
- 35 Lee, D. Y., Um, J., Paneru, G. & Pak, H. K. An experimentally-achieved information-driven Brownian motor shows maximum power at the relaxation time. *Sci Rep-Uk* **8**, 12121, doi:10.1038/s41598-018-30495-6 (2018).
- 36 Albay, J. A. C., Paneru, G., Pak, H. K. & Jun, Y. Optical tweezers as a mathematically driven spatio-temporal potential generator. *Opt Express* **26**, 29906-29915, doi:10.1364/OE.26.029906 (2018).
- 37 Paneru, G., Dutta, S., Sagawa, T., Tlusty, T. & Pak, H. K. Efficiency fluctuations and noise induced refrigerator-to-heater transition in information engines. *Nature Communications* **11**, 1012, doi:10.1038/s41467-020-14823-x (2020).
- 38 Paneru, G., Dutta, S., Tlusty, T. & Pak, H. K. Reaching and violating thermodynamic uncertainty bounds in information engines. *Physical Review E* **102**, 032126, doi:10.1103/PhysRevE.102.032126 (2020).
- 39 Kumar, A. & Bechhoefer, J. Nanoscale virtual potentials using optical tweezers. *Applied Physics Letters* **113**, 183702, doi:10.1063/1.5055580 (2018).
- 40 Luczka, J., Czernik, T. & Hänggi, P. Symmetric white noise can induce directed current in ratchets. *Physical Review E* **56**, 3968-3975, doi:10.1103/PhysRevE.56.3968 (1997).
- 41 Wang, B., Kuo, J., Bae, S. C. & Granick, S. When Brownian diffusion is not Gaussian. *Nature Materials* **11**, 481, doi:10.1038/nmat3308 (2012).
- 42 Ariga, T., Tateishi, K., Tomishige, M. & Mizuno, D. Noise-induced acceleration of single molecule kinesin-1. *arXiv:2012.04214* (2021).
- 43 Ezber, Y., Belyy, V., Can, S. & Yildiz, A. Dynein harnesses active fluctuations of microtubules for faster movement. *Nature Physics* **16**, 312-316, doi:10.1038/s41567-019-0757-4 (2020).
- 44 Paneru, G. & Kyu Pak, H. Colloidal engines for innovative tests of information thermodynamics. *Advances in Physics: X* **5**, 1823880, doi:10.1080/23746149.2020.1823880 (2020).